

## Characterization of *Clostridium thermocellum* strains with disrupted fermentation end-product pathways

Douwe van der Veen · Jonathan Lo · Steven D. Brown · Courtney M. Johnson · Timothy J. Tschaplinski · Madhavi Martin · Nancy L. Engle · Robert A. van den Berg · Aaron D. Argyros · Nicky C. Caiazza · Adam M. Guss · Lee R. Lynd

Received: 27 November 2012 / Accepted: 15 April 2013  
© Society for Industrial Microbiology and Biotechnology 2013

**Abstract** *Clostridium thermocellum* is a thermophilic, cellulolytic anaerobe that is a candidate microorganism for industrial biofuels production. Strains with mutations in genes associated with production of L-lactate (*Aldh*) and/or acetate (*Apta*) were characterized to gain insight into the intracellular processes that convert cellobiose to ethanol and other fermentation end-products. Cellobiose-grown cultures of the *Aldh* strain had identical biomass accumulation, fermentation end-products, transcription profile, and intracellular metabolite concentrations compared to its parent strain (DSM1313 *Δhpt Δspo0A*). The *Apta*-deficient strain grew slower and had 30 % lower final biomass concentration compared to the parent strain, yet produced

75 % more ethanol. A *Aldh Apta* double-mutant strain evolved for faster growth had a growth rate and ethanol yield comparable to the parent strain, whereas its biomass accumulation was comparable to *Apta*. Free amino acids were secreted by all examined strains, with both *Apta* strains secreting higher amounts of alanine, valine, isoleucine, proline, glutamine, and threonine. Valine concentration for *Aldh Apta* reached 5 mM by the end of growth, or 2.7 % of the substrate carbon utilized. These secreted amino acid concentrations correlate with increased intracellular pyruvate concentrations, up to sixfold in the *Apta* and 16-fold in the *Aldh Apta* strain. We hypothesize that the deletions in fermentation end-product pathways result in an intracellular redox imbalance, which the organism attempts to relieve, in part by recycling NADP<sup>+</sup> through increased production of amino acids.

**Electronic supplementary material** The online version of this article (doi:10.1007/s10295-013-1275-5) contains supplementary material, which is available to authorized users.

D. van der Veen · J. Lo · L. R. Lynd (✉)  
Thayer School of Engineering, Dartmouth College,  
Hanover, NH 03755, USA  
e-mail: lee.r.lynd@dartmouth.edu

D. van der Veen  
e-mail: douwevdveen@yahoo.com

D. van der Veen · J. Lo · S. D. Brown ·  
C. M. Johnson · T. J. Tschaplinski · M. Martin ·  
N. L. Engle · A. M. Guss · L. R. Lynd  
BioEnergy Science Center, Oak Ridge, TN 37831, USA

J. Lo  
Department of Biological Sciences, Dartmouth College,  
Hanover, NH 03755, USA

S. D. Brown · C. M. Johnson · T. J. Tschaplinski · M. Martin ·  
N. L. Engle · A. M. Guss  
Biosciences Division, Oak Ridge National Laboratory,  
Oak Ridge, TN 37831, USA

R. A. van den Berg  
Research Group on Quantitative Psychology, Katholieke  
Universiteit Leuven, Tiensestraat 102, 3000 Leuven, Belgium

*Present Address:*  
R. A. van den Berg  
GlaxoSmithKline Vaccines, Rue de l'Institut 89,  
1330 Rixensart, Belgium

A. D. Argyros · N. C. Caiazza · L. R. Lynd  
Mascoma Corporation, Lebanon, NH 03766, USA

*Present Address:*  
N. C. Caiazza  
Synthetic Genomics Inc., 11149 North Torrey Pines Road,  
La Jolla, CA 92037, USA

## Introduction

Increased consumption and progressive depletion of petroleum fossil fuels have led to the development and use of renewable liquid biofuels such as ethanol, for which lignocellulosic biomass is a particularly promising future feedstock [33]. Biological conversion of lignocellulosic biomass to fuels can proceed by using established industrial microorganisms such as yeasts with cellulolytic enzymes either added exogenously or produced heterologously. Alternatively, a microbe with good native capacity to solubilize the carbohydrate fraction of lignocellulose can be engineered for robust industrial fuel production at high yield and titer [6, 24].

The anaerobic thermophilic bacterium *Clostridium thermocellum* is efficient at solubilizing cellulose, especially due to its cell wall-tethered cellulase enzyme complex called the cellulosome [9, 30]. The enzymes of the cellulosome solubilize cellulose to cellobiose, which are taken up and converted by a mixed acid fermentation to ethanol, acetate, L-lactate, formate, hydrogen gas, and carbon dioxide [40].

All known thermophilic saccharolytic anaerobes produce organic acids in addition to ethanol as fermentation end-products. The “classical” approach towards increased ethanol production by rational strain design is to disrupt those metabolic pathways that lead to alternative fermentation end-products such as acetate or lactate, and indeed this strategy has proven successful in some cases. Shaw and coworkers deleted the genes involved in acetate and lactate production in the thermophilic bacterium *Thermoanaerobacterium saccharolyticum* [31]. The resulting *T. saccharolyticum* strain ALK2 had a 50 % increase in ethanol production compared to wild-type levels, while the growth rate of this strain remained comparable to the wild-type strain. Similarly, removal of lactate production in the hemicellulolytic thermophile, *Thermoanaerobacter mathranii*, by disrupting its lactate dehydrogenase (*ldh*) gene, led to increased ethanol production [12]. Lastly, disruption of the lactate dehydrogenase and pyruvate formate lyase pathways in *Geobacillus thermoglucosidasius* also led to improved ethanol yields [5]. However, this “classical” strategy has yet to result in high ethanol yields in the case

of *C. thermocellum* for reasons that are not well understood [1].

Motivated by a desire to increase ethanol yields, we sought to enhance understanding of *C. thermocellum* metabolism by characterizing three mutant strains and comparing them to each other and their parent. The mutant strains had disrupted acetate or L-lactate pathways, which are the major alternative fermentation end-product pathways next to ethanol. We focused especially on these mutants’ growth characteristics and their production of intra- and extracellular metabolites. While the economic feasibility of industrial fermentations relies on the use of cost-effective raw (lignocellulosic) materials, in this study, cellobiose rather than cellulose was used as model carbon source. *C. thermocellum* hydrolyses insoluble cellulose to soluble  $\beta$ -(1,4) linked glucose oligomers including cellobiose. Insoluble substrates interfere with the ability to extract metabolites and monitor real-time fermentation progression (e.g., [18, 22, 29]). As studies comparing cellulose and cellobiose have shown little difference between fermentation end-product distribution [10, 28, 36], and have shown cellobiose to be a good substrate for cellulosome expression [2, 41], the use of cellobiose gives insights on the physiology of these mutants that can serve as starting point for extrapolation to industrial-grade substrates.

## Materials and methods

### Strains

*Clostridium thermocellum* strains used are listed in Table 1. Strains were constructed from the genetically tractable *C. thermocellum* DSM1313 strain [11] following the procedures outlined by Argyros and coworkers [1]. In brief, deletion of the gene encoding the ortholog of the *B. subtilis* *spo0A* sporulation initiation regulator, *spo0A* (Cthe\_0812) in *C. thermocellum*  $\Delta$ *hpt* [1] yielded the  $\Delta$ *hpt*  $\Delta$ *spo0A* genetic background (referred to as the “parent strain”). In this strain, the gene encoding lactate dehydrogenase (*ldh*, Cthe\_1053) was deleted using plasmid pMU1777 [1], removing base pairs +55 to +894 of the

**Table 1** Strains used in this study

Strain name	Genotype	Comment
Parent	<i>Δhpt Δspo0A</i>	Parent strain, derived from <i>C. thermocellum</i> DSM1313 [11]. Strain ID M1726
<i>Δldh</i>	<i>Δhpt Δspo0A Δldh</i>	Deletion of <i>ldh</i> in parent strain. Strain ID M1629
<i>Δpta</i>	<i>Δhpt Δspo0A Δpta</i>	Deletion of <i>pta</i> in parent strain. Strain ID M1630
<i>Δldh Δpta</i>	<i>Δhpt Δspo0A Δldh Δpta</i>	Original merodiploid deletion of <i>pta</i> in strain <i>Δldh</i> . Strain ID M1655
Evolved <i>Δldh Δpta</i>	<i>Δhpt Δspo0A Δldh Δpta</i>	Evolved from <i>Δldh Δpta</i> strain in chemostat for over 500 h. Strain ID M1725

954-bp gene. Similarly, phosphotransacetylase (*pta*, Cthe\_1029) was deleted in *Δhpt Δspo0A* using pMU1817 [1], removing base pairs +174 to +1,074 of the 1,077 bp gene. To make a strain inactivated for both Ldh and Pta, strain *Δhpt Δspo0A Δldh* was transformed with pMU1817, followed by selection on rich medium supplemented with thiamphenicol and 5-fluoro-2'-deoxy-uridine as previously described [1]. Thus, a merodiploid strain was created in which the last 253 base pairs of the *pta* gene were replaced by a *cat*-positive selection marker expressed by a 527-bp *Gapdh* (Cthe\_0137) promoter region. This deletion effectively removed the enzyme's catalytic site, including the catalytically essential Ser<sup>334</sup> and Asp<sup>341</sup> residues in the Pta active site, and Arg<sup>335</sup> that interacts with acetyl-phosphate, as was deduced from sequence alignment with Pta proteins for which crystal structures and structure-function studies are available [20, 37]. Functional disruption of phosphotransacetylase activity in this strain was confirmed by the absence of acetate production in serum bottle fermentations. All gene deletions were confirmed by sequencing the chromosomal locus. As *Δldh Δpta* strains have a severe growth defect [36], the merodiploid *Δldh Δpta* strain was evolved for over 500 h in a chemostat to select for a strain with improved growth rate, yielding the evolved *Δldh Δpta* strain used in this study.

## Fermentation

MTC medium [39] was prepared as previously described [15] with all components except vitamins and trace elements prepared fresh as stock solutions 1 day prior to each fermentation run. Stock solutions were filter-sterilized over 0.22- $\mu$ m cellulose-acetate filters, aliquoted into sterilized, rubber-sealed, N<sub>2</sub>-purged bottles, and stored in the dark until use.

Standardized inoculum was obtained to minimize the impact of differences in inoculum quality on fermentation consistency. At the start of this study, each strain was grown in a 1-l glass fermentor with MTC medium and 5 g/l cellobiose. When an optical density of 0.4 AU was measured with in-vessel probes (Dasgip BioTools, Shrewsbury, MA, USA), 5-ml aliquots were removed from the fermentor vessel, injected into sterile, N<sub>2</sub>-purged, rubber-sealed glass bottles, and stored at -80 °C until use.

Glass 0.5-l fermentors containing 400 ml resazurin-containing water were autoclaved and were allowed to cool to room temperature while the headspace was purged with 10 ml/min N<sub>2</sub> gas for at least 12 h. Three hours before inoculation time, 5-ml aliquots of frozen standardized inoculum were placed on ice and allowed to thaw. Meanwhile, the fermentor vessels were heated to 55 °C, while each fermentor off-gas cooler was kept at 4 °C. At 1 h before inoculation, cellobiose and MTC medium components

were added to each vessel to obtain a working volume of 500 ml. pH was set to 7.2 using 4 M KOH and 1 M H<sub>2</sub>SO<sub>4</sub>. The time of inoculation was designated as time = 0. Optical density was followed by in-vessel probes. Cessation of cellobiose utilization ("maximum OD time point") was determined by both observing the optical density maximum as well as a discontinued addition of base to the vessel.

Prior to each sampling, a 3-ml aliquot was removed and discarded to clear the sampling tube. At an optical density of 0.40  $\pm$  0.05 AU or within 5 min after reaching maximum optical density, which was determined by visually monitoring the continuous OD measurement, 2  $\times$  50-ml broth aliquots were removed from the vessel and centrifuged (5 min, 3,500 $\times$ g), followed by the removal of supernatant using a tube connected to a vacuum pump. Subsequently, pellets were snap-frozen in liquid N<sub>2</sub> and stored at -80 °C until analysis. For any other sampling time point, a 3-ml sample was removed and centrifuged 2 min at 10,000 $\times$ g (3 min for the evolved *Δldh Δpta* strain), followed by decanting and snap-freezing.

## Cell dry weight and total organic carbon and nitrogen (TOCN) analysis

Cell dry weight was determined by taking three 5-ml volumes for each sampling time point, which were filtered over 0.22- $\mu$ m GTTP membranes. Membranes were washed once with 5 ml of water and placed in a 60 °C oven for 5 days, after which the amount of residue was determined.

Total organic carbon and nitrogen (TOCN) content was determined from three 1-ml samples derived from one 5-ml sample volume. Each 1-ml sample was centrifuged (2 min, 10,000 $\times$ g), and 850  $\mu$ l was removed to determine supernatant TOCN values. The pellet was resuspended in 1.0 ml of water and centrifuged three times to remove any remaining supernatant. After washing, the resuspended pellet was added to a TOCN vial containing 9.0 g of distilled water. The vials were analyzed by a TOC-V CPH and TNM-I analyzer (Shimadzu, Kyoto, Japan) operated by TOC-Control V software. As standard solution, 0.5111 g glycine and 8.333 ml of 6 M HCl per liter of distilled water was used in 1, 10, and 50 times dilution. As carrier solvent, 8.72 mM HCl in distilled water was used. The resulting peak area was translated to TOCN values using the standard values in Microsoft Excel.

## Enzymatic analysis

All assays were performed under anaerobic conditions at 50 °C. Cell-free extracts were prepared following methods described in [3]. Briefly, strains were grown in half-liter cultures to O.D. 0.6, chilled, spun down, and resuspended in 4 ml of 100 mM Tris-HCl (pH 7.6), 0.1 mM DTT

buffer. Cells were then disrupted with a sonicator using a microtip. Crude cell extract was centrifuged at  $20,000\times g$  for 10 min, and supernatant was stored on ice. Protein content of the cell extract was determined using the Bradford assay. Reactions were monitored with an Agilent 8453 UV–Vis spectrophotometer with 1 ml of reaction solution.

Phosphotransacetylase and lactate dehydrogenase activity was measured based on previously described methods, following the change in absorbance at 233 nm by thioester bond formation of acetyl-CoA ( $\epsilon = 4,360 \text{ M}^{-1} \text{ cm}^{-1}$ ) and at 339 nm by the oxidation of NADH ( $\epsilon = 6,220 \text{ M}^{-1} \text{ cm}^{-1}$ ), respectively [17, 18]. The reaction conditions for phosphotransacetylase were as follows: 100 mM Tris–HCl pH 7.6, 1.6 mM glutathione, 0.43 mM coenzyme-A, 7.23 mM acetyl phosphate, 13.3 mM ammonium sulphate; and for lactate dehydrogenase 200 mM Tris–HCl pH 7.6, 6.6 mM NADH, 30 mM sodium pyruvate, 1 mM fructose 1,6-diphosphate.

#### Extracellular metabolite analysis

Supernatant obtained after centrifugation was filtered over a 0.22- $\mu\text{m}$  filter spin-column for 2 min at  $10,000\times g$  (3 min for the evolved *Aldh Apta* strain) and stored at  $-20^\circ\text{C}$  until use. Fermentation products were determined by HPLC using an Aminex HPX-87H column (Bio-Rad, Hercules, CA, USA). Extracellular amino acid concentrations were determined by Aminoacids.com (St. Paul, MN, USA).

Lactic acid chirality was determined spectrophotometrically from 100  $\mu\text{l}$  of supernatant using the K-DLATE 05/11 enzyme assay kit (Megazyme, Ireland), following the manufacturer's specifications.

#### Intracellular metabolite analysis

Frozen cell pellet from a 50-ml sample was dissolved in 10 ml of 80% (v/v) aqueous ethanol to which 200  $\mu\text{l}$  of 1,000 g/l D-sorbitol was added. Sorbitol was used as an internal standard to correct for differences in derivatization efficiency and changes in sample volume during heating. This suspension was transferred to a 30-ml Pyrex glass beaker (Corning), placed on ice, and sonicated with a S4000 sonicator (QSonica) using as parameters: tip diameter 12.7 mm, amplitude 120  $\mu\text{m}$ , five series of a 30-s pulse with 30 % amplitude (17 W) followed by 30 s rest. The sonicated suspension was transferred to a 15-ml polypropylene tube and stored at  $-20^\circ\text{C}$  until centrifugation. To remove cell debris, the tubes were centrifuged (5 min,  $3,500\times g$ ) and extraction solvent was carefully transferred to new tubes. The solvent containing metabolites was lyophilized by freeze-drying ( $-50^\circ\text{C}$ , 10 Pa) and stored at  $-80^\circ\text{C}$ .

Five replicate samples were analyzed per microbial strain per time point. Dried extracts were processed as described previously [38] on an inert XL gas chromatograph-mass spectrometer (model 5975C, Agilent Technologies Inc, Santa Clara, CA, USA) with a helium flow of 1.33 ml per minute, and temperatures for the injection port, MS Source, and MS Quad set to 250, 230, and  $150^\circ\text{C}$ , respectively.

#### Data analysis

Cell pellet for the evolved *Aldh Apta* strain proved very loose and unstable, which made supernatant removal after centrifugation difficult. As a result, accurate biomass concentration determination by weight was impossible, and raw measured concentrations data were reported in grams of intracellular compound per volume fermentation broth (Supplementary Data File 1). Intracellular metabolite concentrations were normalized to the pellet nitrogen (TN) present as pellet nitrogen was found to be an accurate proxy for cell biomass (Holwerda et al., manuscript in preparation). This allowed us to calculate a molar concentration of metabolites per gram organic nitrogen biomass (Table 3; Supplementary Data File 1).

For all identified metabolites, the resulting molar concentrations of metabolite per gram organic nitrogen biomass were examined for significance in *R* [27] using two-way ANOVA (response variate: “molar concentration”, classifying variates: “strain” and “timepoint”;  $p = 0.01$ ; results are in Supplementary Data File 1).

## Results

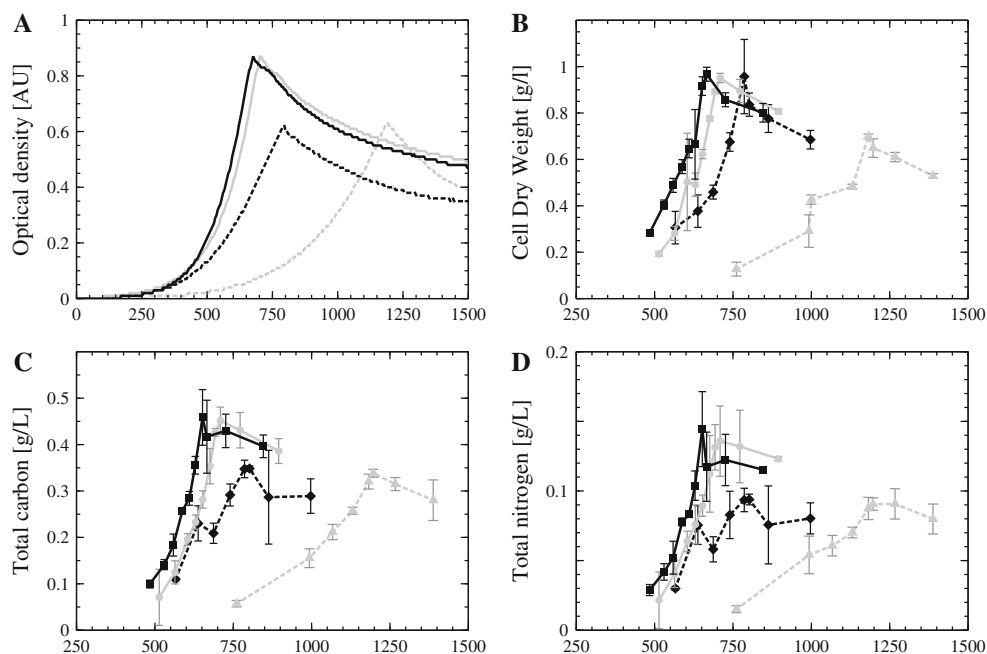
#### Growth characteristics

Growth curves were obtained in pH-controlled bioreactors for strains of *C. thermocellum* DSM1313 with deletions in genes encoding lactate dehydrogenase (*Aldh*), phosphotransacetylase (*Apta*), or both (evolved *Aldh Apta*).

Growth of the *Aldh* strain was not discernibly different from the parent strain, as indicated by the optical density, cell dry weight (CDW), and elemental analysis for carbon and nitrogen (TOC/N) measurements (Fig. 1). Disruption of the *pta* gene alone, however, resulted in slower cell growth, an extended lag phase, and a 30 % decrease in total biomass accumulated during fermentation:  $0.7 \text{ g} \times \text{l}^{-1}$  CDW versus  $1.0 \text{ g} \times \text{l}^{-1}$  CDW for the parent strain, the *ldh* strain, and the evolved *ldh pta* strain.

A strain in which both *ldh* and *pta* were inactivated grew very poorly in glass bottles, and we were unable to initiate growth in a bioreactor. Hence, we examined a chemostat-evolved descendant of this strain selected for improved

**Fig. 1** Growth characteristics. **a** Optical density as measured during one fermentation run, and **b** cell dry weight, **c** total organic carbon in pellet fraction, and **d** total nitrogen in pellet fraction as determined at selected O.D. increments. Parent strain: *solid black line and square*; *Aldh*: *solid gray line and circle*; *Apta*, *dotted gray line and triangle*; evolved *Aldh Apta*, *dotted black line and diamond*. X axis: time in minutes after inoculation. Error bars denote standard error of the mean as determined from three replicate measurements per sampling time point



growth rate. The supernatant of this evolved *Aldh Apta* strain had a higher apparent viscosity: centrifugation times had to be increased to up to 3 min to collect all dialysate per sampling time point. Its CDW was similar to that of the parent strain at  $1.0 \text{ g} \times \text{l}^{-1}$ , yet its TOC/TN and optical density values followed those of the *Apta* strain (Fig. 1). The higher viscosity, lower TOC/TN values, and lower optical density of the *Aldh Apta* strain indicates that additional organic matter is present in its supernatant that is retained in the CDW filtration step, but is not pelleted with the cells upon centrifugation.

Fermentation end-products

Extracellular fermentation end-product concentrations for the examined strains are listed in Table 2. Despite its longer lag phase and lower biomass yield, almost 75 %

more ethanol is produced by the *Apta* strain compared to the three other strains: 17 mM ethanol compared to around 11 mM ethanol, which correspond to 29 and 19 % of theoretical yields, respectively.

Small but significant quantities of lactic acid and acetic acid are detected in the fermentation broth of strains harboring disruptions in these pathways (Table 2). This production of small amounts of lactate and acetate by *ldh* and *pta* mutant strains is consistent with previous reports [1, 36]. To exclude the possible presence of wild-type cells in our inoculum that could explain these small quantities of acetate and lactate, genomic DNA was extracted from cells harvested after a fermentation run. The *ldh* and *pta* regions were amplified by PCR and the resulting amplicons were sequenced. No wild-type DNA sequences but only the expected disrupted nucleotide sequences were found for all strains.

**Table 2** Fermentation end-products

Strain	O.D.	Time point (min) <sup>a</sup>	Cellobiose (mM) <sup>b</sup>	Ethanol (mM) <sup>b</sup>	Acetic acid (mM) <sup>b</sup>	L-lactic acid (mM) <sup>b</sup>	Formate (mM) <sup>b</sup>
Parent	0.4	650 ± 94	8.5 ± 0.8	4.5 ± 1.4	4.7 ± 0.5	0.1 ± 0.0	1.7 ± 0.2
	Maximum	756 ± 92	0.0 ± 0.0	9.7 ± 1.3	10.7 ± 0.5	0.3 ± 0.0	4.5 ± 0.6
<i>Aldh</i>	0.4	582 ± 34	8.8 ± 1.9	3.9 ± 0.6	4.7 ± 0.7	0.1 ± 0.0	1.9 ± 0.3
	Maximum	693 ± 30	0.0 ± 0.0	10.9 ± 2.5	11.6 ± 1.7	0.2 ± 0.0	5.2 ± 0.8
<i>Apta</i>	0.4	1,174 ± 94	5.6 ± 1.1	10.3 ± 1.3	0.3 ± 0.1	0.3 ± 0.1	0.7 ± 0.1
	Maximum	1,313 ± 64	0.0 ± 0.0	16.9 ± 1.2	0.5 ± 0.1	0.7 ± 0.2	1.1 ± 0.2
Evolved <i>Aldh Apta</i>	0.4	705 ± 32	6.6 ± 1.5	5.0 ± 0.4	0.4 ± 0.1	0.3 ± 0.0	0.5 ± 0.1
	Maximum	823 ± 30	0.6 ± 1.0	11.5 ± 3.5	0.7 ± 0.1	0.6 ± 0.1	1.0 ± 0.2

<sup>a</sup> Time in minutes after inoculation of the fermentor vessel

<sup>b</sup> Each value is given as mean with standard deviation as calculated from nine independent biological replicate fermentations for the parent strain and from six independent biological replicate fermentations for the other strains

Lactic acid was formed by both *Aldh* strains, with the evolved double-knockout strain producing up to 0.6 mM lactic acid (Table 2). Whereas in both *ldh*<sup>+</sup> strains, lactate was detected approximately 90 min after acetate was first detected in a fermentor run, in both *Aldh* strains lactate and acetate reached detection threshold concentrations at the same time.

A chirality-specific enzyme assay showed that only L-lactic acid but no D-lactic acid was present in broth samples from all four strains. L-Lactate dehydrogenase enzyme activity was measured in cell-free extracts of the parent strain and the evolved *Aldh Δpta* strain either with or without the addition of fructose 1,6-diphosphate, a known activating molecule for *C. thermocellum* Ldh [19, 25]. Parent strain-specific activity was 0.09 μmol/min per mg protein without fructose 1,6-diphosphate addition, which elevated to 0.69 μmol/min/mg after fructose 1,6-diphosphate addition. For the evolved *Aldh Δpta* strain, specific activity was 0.08 μmol/min per mg protein irrespective of fructose 1,6 diphosphate addition.

In addition to unexpected L-lactic acid production, acetate concentrations to up to 0.7 mM (8 % of parent strain levels) were observed in the *Δpta* and *Aldh Δpta* backgrounds. To verify the functional disruption of *pta*, phosphate acetyltransferase activity was measured in the parent strain and the evolved *Aldh Δpta* strain. While the parent strain had a specific activity of 0.39 μmol/min per mg protein, no phosphate acetyltransferase specific activity could be detected in cell-free extracts of the evolved *Aldh Δpta* strain.

#### Intracellular metabolites

The concentrations of intracellular metabolites in the strains compared in this study were examined by GC–MS. Thirty-nine chromatography peaks with their raw GC-MS peak area differing by at least twofold between any two strains were identified, of which 22 could be assigned to known compounds (Table 3 and Supplementary Data File 1).

The intracellular concentrations of all identified compounds except malic acid were statistically significant different at  $p = 0.01$  between the strains examined in this study (Supplementary Data File 1). Especially at the early exponential growth phase time point, concentration differences were noticeable (Table 3). For example, glucose-6-phosphate and fructose-6-phosphate levels in the two strains harboring the *pta* disruption were 3–6-fold lower compared to those in the parent strain or the *Aldh* strain, and urea concentrations were up to twofold higher in the *Aldh Δpta* strain relative to the three other strains.

Clear differences were observed between the two time points at which the strains were sampled. Intracellular

cellobiose concentrations dropped from around 50–150 μmol × g biomass<sup>-1</sup> in early exponential growth phase to around 2 μmol × g biomass<sup>-1</sup> at the onset of stationary phase. A drop of 2–10-fold over time was observed for the phosphorylytically cleaved products of cellobiose, glucose, and glucose-1-phosphate, as well as for the glycolytic intermediates glucose-6-phosphate, fructose-6-phosphate, and 3-phosphoglycerate (Table 3).

Intracellular pyruvate concentrations decreased over time about threefold in the parental and *Aldh* strains, in line with the other glycolytic intermediates observed. However, the pyruvate concentration did not decrease in the *Δpta* strain, and was over twofold higher in the evolved *Aldh Δpta* strain. Pyruvate serves as a precursor for the synthesis of the amino acid alanine and for the branched-chain amino acids valine, isoleucine, and (when combined with acetyl-CoA) leucine. Similar to pyruvate, the intracellular concentrations of alanine, valine and isoleucine were elevated in the *Δpta* strain and even more so in the evolved *Aldh Δpta* double knockout.

#### Secretion of amino acids

Although all strains studied secrete free amino acids into the fermentation broth, the *Δpta* and *Aldh Δpta* strains secrete substantially more than the parent strain (Table 4). For example, in its early exponential growth phase, the parent strain has secreted 0.6 mM valine, which corresponds to 5 % of the cellobiose carbon consumed. At the onset of stationary phase, its valine concentration increased to 1.2 mM (or 4 % of the cellobiose added on C-mol-basis), and four additional amino acids are present in concentrations above 0.1 mM (Table 4).

Compared to the parent strain, both *Δpta* mutants secreted a subset of amino acids at higher levels. Isoleucine, valine, and alanine concentrations were 1.5 to 2-fold higher in the *Δpta* strain, resulting in 5.8% of the cellobiose carbon converted to free amino acids. In the evolved *Aldh Δpta* strain, these amino acids were elevated 2 to 5-fold. At maximum optical density, *Aldh Δpta* secreted over 17 % (C-mol) of the carbon initially present as cellobiose as free amino acids, of which valine contributed the bulk (14.2 %, or 145.1 mM) (Table 4).

## Discussion

To extend our current knowledge of metabolic processes that affect ethanol yields in *C. thermocellum*, the physiology of strains with a disrupted L-lactate or acetate fermentative pathway or with both these pathways disrupted was examined and compared to their parent strain in bioreactor cultivations on chemically defined minimal

**Table 3** Intracellular metabolite concentrations

Strain	O.D.	Cellobiose	Glucose	Glucose 1-P	Glucose-6-P	Fructose 6-P	3-Phospho-glycerate	Pyruvate	Citric acid	Acornitic acid	Malic acid	Lactic acid
Parent	0.4	84.93 ± 18.8	10.74 ± 1.7	0.17 ± 0.1	6.22 ± 2.5	0.95 ± 0.1	0.63 ± 0.3	1.03 ± 0.2	191.02 ± 58.5	0.47 ± 0.1	0.71 ± 0.1	5.51 ± 4.6
	Maximum	2.08 ± 0.4	10.05 ± 2.5	0.07 ± 0.0	0.63 ± 0.5	0.21 ± 0.1	0.11 ± 0.0	0.36 ± 0.1	135.21 ± 53.8	0.31 ± 0.1	1.05 ± 0.4	3.53 ± 0.6
<i>Aldh</i>	0.4	117.56 ± 48.3	11.16 ± 2.2	0.17 ± 0.0	7.37 ± 2.1	1.03 ± 0.2	0.49 ± 0.2	1.27 ± 0.2	179.49 ± 57.2	0.94 ± 0.3	0.94 ± 0.4	4.72 ± 3.7
	Maximum	2.47 ± 0.5	6.87 ± 1.5	0.08 ± 0.0	0.65 ± 0.5	0.20 ± 0.1	0.11 ± 0.0	0.46 ± 0.0	129.36 ± 5.3	0.34 ± 0.1	1.15 ± 0.2	3.26 ± 1.1
<i>Apta</i>	0.4	49.65 ± 9.3	12.06 ± 2.6	0.17 ± 0.1	2.24 ± 0.5	0.46 ± 0.2	1.16 ± 0.3	2.17 ± 0.4	178.47 ± 58.2	0.76 ± 0.2	1.18 ± 0.3	6.61 ± 2.0
	Maximum	2.82 ± 1.0	10.87 ± 1.8	0.14 ± 0.0	0.84 ± 0.6	0.26 ± 0.1	0.22 ± 0.0	2.57 ± 2.1	162.19 ± 23.9	0.49 ± 0.1	0.93 ± 0.5	7.70 ± 0.8
Evolved <i>Aldh</i>	0.4	143.83 ± 33.3	15.00 ± 4.3	0.27 ± 0.1	1.17 ± 0.5	0.37 ± 0.2	0.56 ± 0.2	2.82 ± 0.5	318.91 ± 45.0	1.31 ± 0.4	0.62 ± 0.1	6.76 ± 2.1
	Maximum	0.90 ± 0.2	8.02 ± 2.5	0.16 ± 0.1	0.14 ± 0.1	0.11 ± 0.0	0.10 ± 0.0	6.45 ± 3.2	250.77 ± 56.6	0.99 ± 0.4	0.95 ± 0.2	8.90 ± 1.8
Strain	O.D.	Alanine	Valine	Leucine	Isoleucine	Threonine	Aspartic acid	Urea	Ornithine	Glycerol-1-P	Palmitic acid	Phosphate
Parent	0.4	2.13 ± 0.5	4.81 ± 1.3	0.63 ± 0.1	0.38 ± 0.1	0.27 ± 0.1	0.39 ± 0.1	507.50 ± 113.7	0.07 ± 0.0	22.24 ± 5.8	8.18 ± 0.8	150.60 ± 40.0
	Maximum	3.01 ± 0.6	9.73 ± 3.3	0.30 ± 0.0	0.57 ± 0.3	0.19 ± 0.0	0.59 ± 0.1	539.94 ± 97.4	0.07 ± 0.0	28.13 ± 3.4	3.98 ± 0.5	53.93 ± 6.4
<i>Aldh</i>	0.4	0.92 ± 0.2	1.33 ± 0.2	0.66 ± 0.1	0.19 ± 0.1	0.59 ± 0.2	0.12 ± 0.0	508.13 ± 133.3	0.07 ± 0.0	31.91 ± 8.6	10.45 ± 4.0	147.18 ± 34.2
	Maximum	1.11 ± 0.3	1.91 ± 0.5	0.27 ± 0.1	0.15 ± 0.1	0.78 ± 0.1	0.12 ± 0.0	443.72 ± 53.9	0.07 ± 0.0	32.45 ± 3.0	5.30 ± 0.8	46.59 ± 1.8
<i>Apta</i>	0.4	1.90 ± 1.1	3.03 ± 1.8	0.71 ± 0.1	0.23 ± 0.1	0.28 ± 0.0	0.28 ± 0.1	444.07 ± 125.4	0.07 ± 0.0	18.79 ± 6.4	7.44 ± 2.1	151.89 ± 18.3
	Maximum	3.32 ± 0.9	4.28 ± 0.4	0.43 ± 0.0	0.23 ± 0.1	0.31 ± 0.1	0.34 ± 0.2	433.21 ± 88.7	0.13 ± 0.0	21.65 ± 5.1	4.73 ± 0.2	105.46 ± 10.3
Evolved <i>Aldh</i> <i>Apta</i>	0.4	2.06 ± 0.4	15.01 ± 6.6	0.52 ± 0.1	0.92 ± 0.5	0.42 ± 0.1	0.45 ± 0.2	868.35 ± 216.5	0.07 ± 0.1	4.11 ± 0.8	8.94 ± 1.1	219.24 ± 27.0
	Maximum	4.77 ± 1.0	43.93 ± 9.8	0.39 ± 0.1	2.02 ± 0.4	0.35 ± 0.2	0.33 ± 0.1	644.20 ± 173.1	0.03 ± 0.0	2.70 ± 0.7	6.59 ± 1.3	147.56 ± 35.0

Concentrations in µmol per gram total nitrogen (TN) biomass. Values are the average and standard deviation of five independent biological replicate samples per strain per time point

**Table 4** Extracellular amino acids in the fermentation broth

Strain	O.D.	Time Point <sup>a</sup>	Glu (μM)	Gln (μM)	Pro (μM)	Thr (μM)	Ile (μM)	Ala (μM)	Val (μM)	Ser (μM)
Parent	0.4	558	104.4	19.7	46.4	n.d.	52.5	47.5	563.1	37.3
	Maximum	684	153.1	51.0	136.7	18.3	129.4	141.0	1,200.7	49.4
<i>Aldh</i>	0.4	610	70.6	13.4	42.8	n.d.	51.3	44.3	403.8	32.9
	Maximum	714	122.7	27.1	127.4	n.d.	125.4	117.3	1,105.7	46.2
<i>Apta</i>	0.4	1,174	75.1	25.9	n.d.	16.7	114.3	96.2	861.9	47.4
	Maximum	1,297	105.7	33.6	70.4	27.3	194.5	171.0	1,625.6	51.6
Evolved <i>Aldh Apta</i>	0.4	753	58.8	34.9	76.9	34.6	466.6	82.2	2,249.7	25.2
	Maximum	871	111.2	64.8	154.2	69.2	839.6	182.1	5,077.0	32.9

Only amino acids for which a concentration over 50 μM in at least one sample is detected are presented. Asp, Leu, Gly, and Phe are detected at concentrations below 50 μM. Arg, Asx, Met, Lys, Tyr, Trp, and His were not detected in any sample. Cys cannot be determined with the detection method used. *n.d.* not detected

<sup>a</sup> Time is given in minutes after inoculation of the fermentor vessel

medium with cellobiose as sole carbon source. Independent bioreactor runs for each strain proved highly reproducible, which allowed us to make detailed observations on aspects of *C. thermocellum*'s physiology.

Both L-lactate and acetate were detected in the fermentation broths of strains disrupted for the L-lactate or acetate fermentative pathways. The observed non fructose-1,6-bisphosphate-dependent Ldh activity in *Aldh* strains might be explained by the presence of one or more enzymes that complement this Ldh activity. The putative malate dehydrogenase (Cthe\_0345) is a likely candidate for further investigations in this respect, given its high similarity at the amino acid level with Ldh (BLAST E-value:  $2 \times 10^{-207}$ ), its belonging to the same protein superfamily [23], and the observed shift in substrate specificity from malate to lactate by a single amino acid residue substitution [13].

Disruption of *pta* reduced growth (Fig. 1) yet produced 1.7-fold more ethanol than its parent strain (Table 2). These increased ethanol levels are in line with the approximately 1.3-fold increased ethanol levels of a comparable *pta* strain fermented in bottle flasks on rich medium [36]. Unexpectedly, ethanol levels returned to parent strain levels in the evolved strain in which both *ldh* and *pta* were disrupted. Added to that observation is the presence of unidentified soluble material in this strain's fermentation broth, as is indicated by an increased broth viscosity and by the observed discrepancy between biomass determination by the cell dry weight or TOC/TN procedure. Our observations are in contrast with the almost fourfold-increased ethanol levels that Argyros and coworkers found when working with another evolved *Aldh Apta* strain [1]. Comparison between this latter experiment and ours is not possible, as this latter experiment was performed by bottle flask cultivation grown on rich medium and with 20 g/l Avicel cellulose as carbon source. However, it will be of

interest to compare side-by-side both evolved *Aldh Apta* strains in minimal media on both cellobiose and crystalline cellulose to determine whether media composition or carbon source may account for this observed discrepancy.

Pyruvate is a key intracellular metabolite that plays a role in several metabolic pathways, including cellobiose fermentation [28]. Secretion of pyruvate by *C. thermocellum* was reported earlier for the *Δhpt Aldh Apta* strain described by Argyros and coworkers when it was grown on Avicel cellulose [1]. They observed that secretion of pyruvate disappeared in a strain that was evolved for faster growth. Although in our study extracellular pyruvate concentrations were not determined, intracellular pyruvate concentrations were increased in our *Apta* and evolved *Aldh Apta* strains to up to 16-fold in the latter strain relative to parent strain levels. Correlating with these elevated intracellular pyruvate levels were higher intra- and extracellular levels of free amino acids including pyruvate-derived valine, isoleucine and alanine. In cellulose and cellobiose studies of *C. thermocellum* strain ATCC27405, Ellis and coworkers found that both fermentations converted about 5 % of substrate carbon to secreted amino acids, suggesting that amino acid secretion is not significantly affected by substrate [10]. Under our experimental conditions, all DSM1313-derived strains secrete large quantities of amino acids, with the evolved *Aldh Apta* mutant converting 17% of its initial substrate carbon atoms to free amino acids. Amino acid biosynthesis represents a bioenergetic cost to the cell, as it requires cleavage of high-energy phosphate bonds [4, 35]. Yet, despite these costs, the strains examined in this study divert a significant portion of their metabolic flux towards these pathways, suggesting that this flux fulfills a major metabolic need.

For the mesophile *Clostridium cellulolyticum*, chemostat experiments suggests that its metabolism is adapted to low carbon flows [8, 14, 26]. At such low flows, the NAD<sup>+</sup> that

is reduced by glycolysis can be oxidized through hydrogen gas formation through pyruvate:ferredoxin oxidase activity [14, 26]. However, with increased intracellular carbon flow, this hydrogen gas-mediated  $\text{NAD}^+$  regeneration is not able to keep pace. The resulting imbalanced electron flow causes excess carbon to be passed on through pyruvate to increased lactate production and exopolysaccharide synthesis in this organism [7, 26]. Similar to *C. cellulolyticum*, *C. thermocellum* engineered strains might have an imbalanced electron flow. In this study, the most abundantly secreted amino acids observed (valine, isoleucine, alanine, proline, and glutamate) all require little to no ATP, yet substantial amounts of NADPH for their synthesis (e.g., biosynthesis of 1 mol of valine yields 2 mol of  $\text{NADP}^+$  at no ATP cost, and isoleucine 5 mol of  $\text{NADP}^+$  at the cost of 2 mol of ATP [4, 21]. Thus, the observed flux towards these amino acids might be explained by a need to regenerate  $\text{NADP}^+$  through amino acid biosynthesis. Regeneration of  $\text{NADP}^+$  by production of amino acids has been shown to occur in the fungus *Aspergillus nidulans* under oxygen depletion conditions [32] and in the archaeon *Pyrococcus furiosus* [16]. Furthermore, an extensive study involving 135 anaerobic rumen bacteria suggested that most of these bacteria secreted amino acids, the highest levels of which were those that require NADPH for their biosynthesis yet have low ATP cost [34].

Our study suggests that not-well-understood metabolic processes redirect carbon not towards ethanol, but through other pathways, notably amino acid biosynthetic pathways. As the amino acids with highest concentrations are synthesized with high NADPH consumption, this diversion might be because of an imbalanced cellular redox state of *C. thermocellum*. It appears of paramount importance that a better understanding of this cellular redox state is required for further successful engineering of improved ethanol yields of this organism. Future experiments that investigate differences in intracellular metabolism between cellulose- and cellobiose-grown cultures should give further clues about the (redox state) processes that underlie this observed secretion of amino acids. In addition, experiments that compare side-by-side various evolved *C. thermocellum* mutant strains will likely identify mutations that modify pathways involved in improved growth, carbon, and electron flow in *C. thermocellum*.

**Acknowledgments** This work was supported by the Office of Biological and Environmental Research in the DOE Office of Science through the BioEnergy Science Center, a U.S. DOE Bioenergy Research Center. Oak Ridge National Laboratory is managed by UT-Battelle, LLC, for the U.S. Department of Energy under contract DE-AC05-00OR22725. We would like to thank Mascoma Corporation, Lebanon, NH, for the use of strains used in this study, Marybeth I. Maloney for performing DNA sequencing, and Kyle D. Hirst for performing the TOC/TN analysis.

## References

- Argyros DA, Tripathi SA, Barrett TF, Rogers SR, Feinberg LF, Olson DG, Foden JM, Miller BB, Lynd LR, Hogsett DA, Caiazza NC (2011) High ethanol titers from cellulose by using metabolically engineered thermophilic, anaerobic microbes. *Appl Environ Microbiol* 77:8288–8294
- Bhat S, Goodenough PW, Owen E, Bhat MK (1993) Cellobiose: a true inducer of cellulosome in different strains of *Clostridium thermocellum*. *FEMS Microbiol Lett* 111:73–78
- Brown SD, Guss AM, Karpinetz TV, Parks JM, Smolin N, Yang S, Land ML, Klingeman DM, Bhandiwad A, Rodriguez MJ, Raman B, Shao X, Mielenz JR, Smith JC, Keller M, Lynd LR (2011) Mutant alcohol dehydrogenase leads to improved ethanol tolerance in *Clostridium thermocellum*. *Proc Natl Acad Sci USA* 108:13752–13757
- Craig CL, Weber RS (1998) Selection costs of amino acid substitutions in ColE1 and ColIa gene clusters harbored by *Escherichia coli*. *Mol Biol Evol* 15:774–776
- Cripps RE, Eley K, Leak DJ, Rudd B, Taylor M, Todd M, Boakes S, Martin S, Atkinson T (2009) Metabolic engineering of *Geobacillus thermoglucosidasius* for high-yield ethanol production. *Metab Eng* 11:398–408
- Dellomonaco C, Fava F, Gonzalez R (2010) The path to next generation biofuels: successes and challenges in the era of synthetic biology. *Microb Cell Fact* 9:3
- Desvaux M (2006) Unravelling carbon metabolism in anaerobic cellulolytic bacteria. *Biotechnol Prog* 22:1229–1238
- Desvaux M, Guedon E, Petitdemange H (2001) Carbon flux distribution and kinetics of cellulose fermentation in steady-state continuous cultures of *Clostridium cellulolyticum* on a chemically defined medium. *J Bacteriol* 183:119–130
- Ding S, Xu Q, Crowley M, Zeng Y, Nimlos M, Lamed R, Bayer EA, Himmel ME (2008) A biophysical perspective on the cellulosome: new opportunities for biomass conversion. *Curr Opin Biotechnol* 19:218–227
- Ellis LD, Holwerda EK, Hogsett D, Rogers S, Shao X, Tschaplinski T, Thorne P, Lynd LR (2012) Closing the carbon balance for fermentation by *Clostridium thermocellum* (ATCC 27405). *Bioresour Technol* 103:293–299
- Feinberg L, Foden J, Barrett T, Davenport KW, Bruce D, Detter C, Tapia R, Han C, Lapidus A, Lucas S, Cheng J, Pitluck S, Woyke T, Ivanova N, Mikhailova N, Land M, Hauser L, Argyros DA, Goodwin L, Hogsett D, Caiazza N (2011) Complete genome sequence of the cellulolytic thermophile *Clostridium thermocellum* DSM1313. *J Bacteriol* 193:2906–2907
- Georgieva TI, Ahring BK (2007) Evaluation of continuous ethanol fermentation of dilute-acid corn stover hydrolysate using thermophilic anaerobic bacterium *Thermoanaerobacter* BG1L1. *Appl Microbiol Biotechnol* 77:61–68
- Goward CR, Nicholls DJ (1994) Malate dehydrogenase: a model for structure, evolution, and catalysis. *Protein Sci* 3:1883–1888
- Guedon E, Payot S, Desvaux M, Petitdemange H (1999) Carbon and electron flow in *Clostridium cellulolyticum* grown in chemostat culture on synthetic medium. *J Bacteriol* 181:3262–3269
- Holwerda EK, Hirst KD, Lynd LR (2012) A defined growth medium with very low background carbon for culturing *Clostridium thermocellum*. *J Ind Microbiol Biotechnol* 39(6):943–947
- Kengen S, Stams A (1994) Formation of L-alanine as a reduced end product in carbohydrate fermentation by the hyperthermophilic archaeon *Pyrococcus furiosus*. *Arch Microbiol* 161:168–175
- Klotzsch H (1969) Enzymatic assay of phosphotransacetylase (EC 2.3.1.8). *Meth Enzymol* XIII:381–386
- Lamed R, Zeikus JG (1980) Ethanol production by thermophilic bacteria: relationship between fermentation product yields of and

- catabolic enzyme activities in *Clostridium thermocellum* and *Thermoanaerobium brockii*. J Bacteriol 144:569–578
19. Lamed R, Zeikus JG (1981) Thermostable, ammonium-activated malic enzyme of *Clostridium thermocellum*. Biochim Biophys Acta 660:251–255
  20. Lawrence SH, Luther KB, Schindelin H, Ferry JG (2006) Structural and functional studies suggest a catalytic mechanism for the phosphotransacetylase from *Methanosarcina thermophila*. J Bacteriol 188:1143–1154
  21. Lengeler JW, Drews G, Schlegel HG (1999) Biology of the Prokaryotes. Thieme, Stuttgart
  22. Li H, Knutson BL, Nokes SE, Lynn BC, Flythe MD (2012) Metabolic control of *Clostridium thermocellum* via inhibition of hydrogenase activity and the glucose transport rate. Appl Microbiol Biotechnol
  23. Madern D (2002) Molecular evolution within the L-malate and L-lactate dehydrogenase super-family. J Mol Evol 54:825–840
  24. Olson DG, McBride JE, Joe Shaw A, Lynd LR (2012) Recent progress in consolidated bioprocessing. Curr Opin Biotechnol 23(3):396–405
  25. Ozkan M, Yilmaz EI, Lynd LR, Ozcengiz G (2004) Cloning and expression of the *Clostridium thermocellum* L-lactate dehydrogenase gene in *Escherichia coli* and enzyme characterization. Can J Microbiol 50:845–851
  26. Payot S, Guedon E, Cailliez C, Gelhaye E, Petitdemange H (1998) Metabolism of cellobiose by *Clostridium cellulolyticum* growing in continuous culture: evidence for decreased NADH reoxidation as a factor limiting growth. Microbiology 144:375–384
  27. R Development Core Team (2011) R: a language and environment for statistical computing. R Foundation for Statistical Computing, Vienna. ISBN 3-900051-07-0
  28. Rydzak T, Levin DB, Cicek N, Sparling R (2011) End-product induced metabolic shifts in *Clostridium thermocellum* ATCC 27405. Appl Microbiol Biotechnol 92:199–209
  29. Rydzak T, McQueen PD, Krokhin OV, Spicer V, Ezzati P, Dwivedi RC, Shamshurin D, Levin DB, Wilkins JA, Sparling R (2012) Proteomic analysis of *Clostridium thermocellum* core metabolism: relative protein expression profiles and growth phase-dependent changes in protein expression. BMC Microbiol 12:214
  30. Schwarz WH (2001) The cellulosome and cellulose degradation by anaerobic bacteria. Appl Microbiol Biotechnol 56:634–649
  31. Shaw AJ, Podkaminer KK, Desai SG, Bardsley JS, Rogers SR, Thorne PG, Hogsett DA, Lynd LR (2008) Metabolic engineering of a thermophilic bacterium to produce ethanol at high yield. Proc Natl Acad Sci USA 105:13769–13774
  32. Shimizu M, Fujii T, Masuo S, Takaya N (2010) Mechanism of de novo branched-chain amino acid synthesis as an alternative electron sink in hypoxic *Aspergillus nidulans* cells. Appl Environ Microbiol 76:1507–1515
  33. Somerville C, Youngs H, Taylor C, Davis SC, Long SP (2010) Feedstocks for lignocellulosic biofuels. Science 329:790–792
  34. Stevenson IL (1978) The production of extracellular amino acids by rumen bacteria. Can J Microbiol 24:1236–1241
  35. Stryer L (1995) Biochemistry, 4th edn. W.H. Freeman and Company, New York
  36. Tripathi SA, Olson DG, Argyros DA, Miller BB, Barrett TF, Murphy DM, McCool JD, Warner AK, Rajgarhia VB, Lynd LR, Hogsett DA, Caiazza NC (2010) Development of pyrF-based genetic system for targeted gene deletion in *Clostridium thermocellum* and creation of a pta mutant. Appl Environ Microbiol 79:6591–6599
  37. Xu QS, Jancarik J, Lou Y, Kuznetsova K, Yakunin AF, Yokota H, Adams P, Kim R, Kim S (2005) Crystal structures of a phosphotransacetylase from *Bacillus subtilis* and its complex with acetyl phosphate. J Struct Funct Genomics 6:269–279
  38. Yang S, Tschaplinski TJ, Engle NL, Carroll SL, Martin SL, Davison BH, Palumbo AV, Rodriguez MJ, Brown SD (2009) Transcriptomic and metabolomic profiling of *Zymomonas mobilis* during aerobic and anaerobic fermentations. BMC Genomics 10:34
  39. Zhang YP, Lynd LR (2005) Regulation of cellulase synthesis in batch and continuous cultures of *Clostridium thermocellum*. J Bacteriol 187:99–106
  40. Zhang YP, Lynd LR (2005) Cellulose utilization by *Clostridium thermocellum*: bioenergetics and hydrolysis product assimilation. Proc Natl Acad Sci USA 102:7321–7325
  41. Zverlov VV, Schwarz WH (2008) Bacterial cellulose hydrolysis in anaerobic environmental subsystems—*Clostridium thermocellum* and *Clostridium stercorarium*, thermophilic plant-fiber degraders. Ann N Y Acad Sci 1125:298–307